Geotextiles and Geomembranes 28 (2010) 85–92

Contents lists available at ScienceDirect

Geotextiles and Geomembranes

journal homepage: www.elsevier.com/locate/geotexmem

A simplified two-phase macroscopic model for reinforced soils

Ehsan Seyedi Hosseininia*, Orang Farzaneh

School of Civil Engineering, Faculty of Engineering, University of Tehran, Shanzdah Azar Avenue, Enghelab Street, P.O. Box: 14155-6457, Tehran, Iran

ARTICLE INFO

Article history:
Received 22 November 2008
Received in revised form
20 July 2009
Accepted 22 September 2009
Available online 11 December 2009

Keywords:
Interface
Reinforced soil
Multiphase model
Numerical analysis

ABSTRACT

This paper presents the formulation of a macroscopic model for reinforced soil structures in which the interface is taken into consideration as a rigid-plastic contact. The model is formulated in the framework of a so-called multiphase model recently introduced for reinforced soil masses. The proposed simplified two-phase model can be considered as an optimal solution between extremely simplified perfect bonding model on one hand, and using a third phase for the interface on the other hand, which results in a more complicated and time-consuming model. The introduced platform is implemented in a numerical code. The proposed model is evaluated by simulating (a) the failure of laboratorial plane strain compression tests; (b) the behavior of a 1-g reinforced soil retaining wall model under external loading, and (c) the deformation of a reinforced soil structure under its own weight, which has been analyzed by another homogenization approach including elastoplastic interface model. The results indicate that the deformation of reinforced soil structures can be satisfactorily predicted by the proposed model.

1. Introduction

Reinforced soils may be regarded as multilayered composite systems due to the existence of periodic layers of soil and inclusion. The behavior of this systematic material can be analyzed with the aid of homogenization methods, by which an equivalent medium is introduced with a homogenous, but anisotropic behavior in macroscopic view (e.g., de Buhan et al., 1989; Harrison and Gerrard, 1972; Michalowski and Zhao, 1995; Romstad et al., 1976). For reinforced soil medium, de Buhan and Sudret (1999) have recently introduced "Multiphase Model" as an extension of classical homogenization methods, in the sense that the composite is represented at the macroscopic scale not by one single medium as in the homogenization methods, but by superposed mutually interacting media (or "phases"). For instance, in a two-phase system, each geometrical point consists of two coincident particles including matrix phase (representative of soil) and reinforcement phase (representative of inclusion). In the general case, it is possible to dedicate different kinematic fields to each phase relating to each other through an interaction law. Consequently, despite classical homogenization methods, the multiphase model can capture both scale and boundary effects (Ben Hassine et al., 2008).

In the initial introduced multiphase models, it has been supposed that the matrix and reinforcement phases be perfectly bonded to each other. The inclusions were considered as one-dimensional elements. Using this approach, several boundary value problems were studied in the literature. The examples are the analysis of a piled-raft group (de Buhan and Sudret, 2000) and that of a rock-bolted tunnel (Sudret and de Buhan, 2001). The model was further developed by considering flexural (de Buhan and Sudret, 2000) and shear behaviors (Hassen and de Buhan, 2005) of such linear inclusions. In all these analyses, the matrix phase has been taken as a linear elastic–perfectly plastic material. More recently, the applicability of inelastic non-linearity in the behavior of soil is paid attention and the behavior of reinforced soil systems have been simulated and evaluated (Seyedi Hosseininia, 2009; Seyedi Hosseininia and Farzaneh, 2007, 2008).

The perfect bonding between soil and inclusion does not always exist. In a reinforced soil wall, for example, the interface might have a weaker strength than soil–soil contact that influences the global wall behavior. As a matter of fact, the performance of soil-structure systems depends on not only the behavior of each constituent, but also on the interaction between soil and inclusions, which is stabilized through interface behavior. Hence, the multiphase model was then developed in such a way that the "interface phase" was introduced in which, an interaction force was related to relative displacement between phases. Bennis and de Buhan (2003) calculated the settlement of a piled-raft foundation with/without interface phase. Similarly, Thai et al. (2009) have studied numerically the stability of a reinforced retaining wall and compared the results with

* Corresponding author. Tel.: +98 9122263498; fax: +98 2166403808.
E-mail addresses: eseyedi@ut.ac.ir (E.S. Hosseininia), ofarzane@ut.ac.ir (O. Farzaneh).

0266-1144/$ – see front matter © 2009 Elsevier Ltd. All rights reserved.
doi:10.1016/j.geotexmem.2009.09.009

those of upper bound limit analysis. It is worth noting that this technique makes the formulation more complicated as well as more time-consuming in comparison with perfect bonding condition. This is because, in one hand, the interface phase has been considered as a new phase existing in each geometrical point, i.e., three superposed phases. On the other hand, the algorithm of such analysis requires the calculation of individual displacement fields of matrix and reinforcement phases based on the interface behavior which either holds the interaction law or reveals the failure condition.

It is interesting to note that the interaction need not always fail due to relative movement of soil and inclusion alone, but sometimes it can also fail because of shear failure of the interface. This case was discussed by Tatsuoka (1985) where the interface failure is only due to the mobilization of maximum shear strength originated from stress rotation axes. Observational investigations in laboratory and field tests indicate the possibility of such failure mechanism in reinforced soil structures (e.g., Cazzuffi et al., 1993; Hatami and Bathurst, 2005, 2006; Kotake et al., 1999; Matichard et al., 1992; Peng et al., 2000).

The objective of this paper is to consider the interface as a rigid-perfectly plastic contact in a two-phase system to simulate soil–inclusion interaction as an optimal solution between overly simplified perfect bonding model on one hand, and having to use the third phase on the other hand, which results in a more complicated and time-consuming model. In the present contribution, the planar inclusions have only tensile behavior. The formulation is expressed in-plane strain condition. By implementing the formulation in a numerical code, the model is evaluated and verified by simulating the behavior of reinforced soil retaining walls.

2. Formulation of a two-phase system

This section briefly deals with the constitutive equations of a perfectly bonded two-phase system for reinforced soils. A detailed explanation can be found in de Buhan and Sudret (1999). The inclusions are assumed bi-dimensional and only support tensile forces.

Consider a granular medium including thin planar inclusions that are placed periodically (Fig. 1a). The inclusions may be laid in an arbitrary direction with an angle α with 1-axis of a global coordinate system (1–2–3). As a consequence, the medium can be regarded, from a macroscopic viewpoint, as a superposition of matrix and reinforcement phases occupying the whole space as shown in Fig. 1b. The sign of compressive stress and strain components is considered as positive.

2.1. Reinforcement phase

The inclusion layers are placed with the same spacing (h) from each other (Fig. 1a). Consider a local Cartesian x–y–z coordinate system in which the plane of inclusion is set in x–y plane. The y-direction shows the out-of-plane direction parallel with the 3-axis of the global coordinate system. The thickness (t) of the inclusion (along z-direction) is assumed to be negligible compared with other dimensions.

The inclusion has a linear elastic–perfectly plastic behavior with Young's modulus (E^{inc}), Poisson's ratio (ν^{inc}) and tensile strength ($\sigma_{\mathrm{u}}^{\mathrm{inc}}$). The corresponding macroscopic parameters with superscript r (E^r,ν^r and σ_u^r) can be defined by a reinforcement volume ratio (χ) which is equal to the volume ratio of the inclusion (V^{inc}) to the soil (V^{s}) in one periodic span (refer to Fig. 1):

$$\chi = \frac{V^{\mathrm{inc}}}{V^{\mathrm{s}}} = \frac{t}{h} \tag{1}$$

Thus, the macroscopic properties of the reinforcement phase (without any change in Poisson's ratio) are as follows:

$$E^r = \chi E^{\mathrm{inc}} \tag{2a}$$

$$\sigma_{\mathrm{u}}^r = \chi \sigma_{\mathrm{u}}^{\mathrm{inc}} \tag{2b}$$

In the macroscopic scale and according to the elasticity theory for bi-dimensional reinforcement phase, we have:

$$\begin{Bmatrix} \Delta\sigma_x^r \\ \Delta\sigma_y^r \end{Bmatrix} = \frac{E^r}{1-\nu^{r2}} \begin{bmatrix} 1 & \nu^r \\ \nu^r & 1 \end{bmatrix} \begin{Bmatrix} \Delta\epsilon_x^r \\ \Delta\epsilon_y^r \end{Bmatrix} \tag{3}$$

where (σ_x^r, σ_y^r) and $(\epsilon_x^r, \epsilon_y^r)$ are in-plane axial stress and strain components, respectively. Hereafter, the sign Δ denotes the increment of the related parameter. Under the condition of plane strain ($\epsilon_z^r = 0$), the two-dimensional stress–strain relationship in Eq. (3) turns into the following simple form:

$$\Delta\sigma_x^r = \left[\frac{E^r}{1-\nu^{r2}}\right]\Delta\epsilon_x^r, \quad \Delta\sigma_y^r = \left[\frac{\nu^r E^r}{1-\nu^{r2}}\right]\Delta\epsilon_x^r \tag{4}$$

Generally, the applied stress on the inclusion surface is too small in comparison with the in-plane stress components (i.e.,$|\sigma_x^r| > |\sigma_y^r| \gg |\sigma_z^r|$); it is a common practice to ignore the contribution of out-of-plane stress in the inclusion behavior. By considering the Tresca yield criterion for the reinforcement phase, the yield function becomes:

$$f^r(\sigma_i^r) = \sigma_x^r - \sigma_u^r \tag{5}$$

2.2. Matrix phase

A linear elastic–perfectly plastic model is considered here for matrix phase behavior. It is obvious that there is no need to reduce soil properties since the inclusion properties have already been scaled to soil volume (Eq. (2)).

The yield function of matrix (f^{m}) is supposed to be the familiar Mohr–Coulomb criterion as follows:

$$f^{\mathrm{m}}(\sigma_I^{\mathrm{m}}, \sigma_{II}^{\mathrm{m}}) = (\sigma_I^{\mathrm{m}} - \sigma_{II}^{\mathrm{m}}) - \sin\phi^{\mathrm{m}}(\sigma_I^{\mathrm{m}} + \sigma_{II}^{\mathrm{m}}) \tag{6}$$

where φ^{m} is the internal friction angle and ($\sigma_{\mathrm{I}}^{\mathrm{m}}$,$\sigma_{\mathrm{II}}^{\mathrm{m}}$) are major and minor principal stresses. The superscript m denotes matrix phase. In a similar way, the plastic potential function (g^m) is defined using the dilation angle (ψ^{m}):

$$g^{\mathrm{m}}(\sigma_I^{\mathrm{m}}, \sigma_{II}^{\mathrm{m}}) = (\sigma_I^{\mathrm{m}} - \sigma_{II}^{\mathrm{m}}) - \sin\psi^{\mathrm{m}}(\sigma_I^{\mathrm{m}} + \sigma_{II}^{\mathrm{m}}) \tag{7}$$

The constitutive relation for soil (and consequently matrix phase) is:

$$\Delta\sigma_{ij}^{\mathrm{m}} = A_{ijkl}^{\mathrm{e}}\left(\Delta\epsilon_{kl}^{\mathrm{m}} - \Delta\epsilon_{kl}^{\mathrm{mp}}\right) \tag{8}$$

in which A_{ijkl}^{e} is elastic stiffness tensor. Plastic strain rate ($\Delta\epsilon_{ij}^{\mathrm{mp}}$) is calculated from the flow rule:

$$\Delta\epsilon_{ij}^{\mathrm{mp}} = <\lambda^{\mathrm{m}}> \frac{\partial g^{\mathrm{m}}}{\partial\sigma_{ij}^{\mathrm{m}}} \tag{9}$$

where λ^{m} is the plastic loading multiplier and we have $<x> = x$ for $x > 0$ and $<x> = 0$, otherwise.

2.3. Assembly of phases in a two-phase system

For any arbitrary geometrical point of a two-phase material, the element is under the influence of global stress components (Σij) as

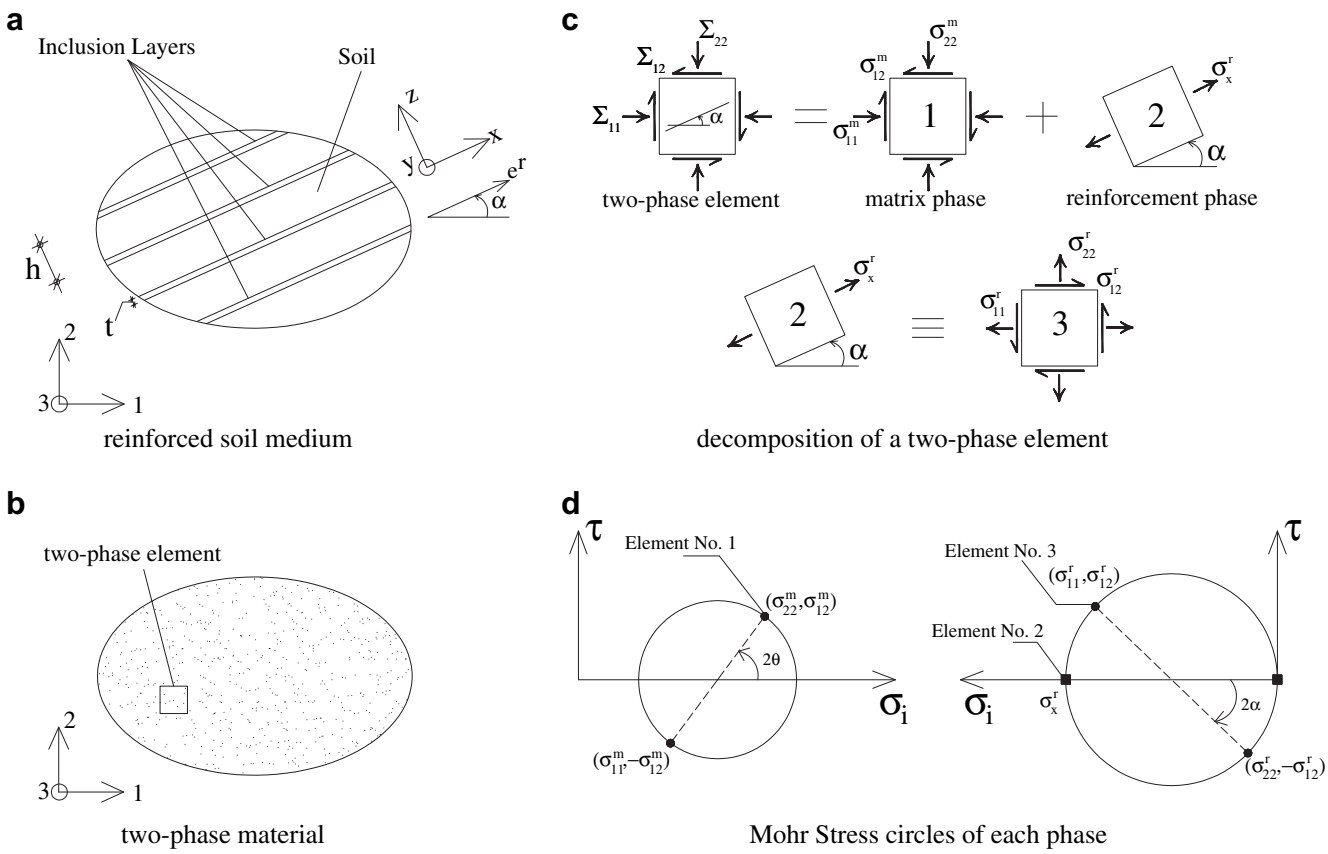

Fig. 1. (a) Microscopic view of a reinforced soil medium including soil and inclusions; (b) Macroscopic view of the reinforced soil medium which is regarded as a two-phase system; (c) A two-phase element is decomposed into matrix and reinforcement phases (d) demonstration of stress state by Mohr stress circles.

shown in Fig. 1c. The two-phase element can be decomposed into matrix and reinforcement phases, which results in distinguishing the stress components of each phase. Despite the matrix phase (element no. 1), the stress in the reinforcement phase consists of only axial component (σ_x^r) along local x direction, as obtained in Eq. (4). Stress equilibrium always exists between phases. In order to consider this equality, the axial stress in the reinforcement (element no. 2) is replaced by its corresponding stress components on the same element which is rotated clockwise with an angle of 2α on the stress Mohr circle (element no. 3). The corresponding stress points are shown in Fig. 1d. The axial stress of the reinforcement phase can be written in a tensor form and thus, stress equilibrium condition is written as follows:

$$\Delta\Sigma_{ij} = \Delta\sigma_{ij}^{\mathrm{m}} + \Delta\sigma_{ij}^{r} = \Delta\sigma_{ij}^{\mathrm{m}} + \Delta\sigma_{x}^{r}\left(e_i^r \otimes e_j^r\right) \tag{10}$$

The symbol $\otimes$ denotes dyadic product of vectors. The unit vector e_i^r shows the direction of inclusion and equals:

$$e_i^r = \{\cos\alpha, \sin\alpha\} \tag{11}$$

According to the hypothesis of perfect bonding, the strain compatibility between phases can be stated as follows:

$$\Delta\in_{ij} = \Delta\varepsilon_{ij}^{\mathrm{m}} = \Delta\varepsilon_{ij}^{r} = \Delta\varepsilon_{x}^{r}\left(e_i^r \otimes e_j^r\right) \tag{12}$$

where $\in_{ij}$ and ε_{ij} denote strain tensors of composite and phases, respectively. Herein, it is important to mention that since the stress and strain tensors of the reinforcement phase have appeared as second order tensors, a fourth order tensor is presented as reinforcement stiffness tensor A_{ijkl}^r in the following form:

$$\Delta\sigma_{ij}^{r} = A_{ijkl}^{r}\Delta\varepsilon_{kl}^{r}, \quad A_{ijkl}^{r} = E^r\left(e_i^r \otimes e_j^r \otimes e_k^r \otimes e_l^r\right) \tag{13}$$

Now, by taking Eq. (12) as well as Eq. (10), the constitutive equation of a two-phase system can be obtained:

$$\begin{aligned}\Delta\in_{ij} &= \Delta\varepsilon_{ij}^{\mathrm{m}} = C_{ijkl}^{\mathrm{m}}\Delta\sigma_{kl}^{m} = C_{ijkl}^{m}\left(\Delta\Sigma_{kl} - \Delta\sigma_{kl}^{r}\right) = C_{ijkl}^{m}\left(\Delta\Sigma_{kl} - A_{ijkl}^{r}\Delta\varepsilon_{kl}^{r}\right)\\ &\Rightarrow \left(\delta_{ij}\delta_{kl} + A_{ijmn}^{r}C_{mnkl}^{\mathrm{ep}}\right)\Delta\in_{ij} = C_{mnkl}^{\mathrm{ep}}\Delta\Sigma_{kl} \Rightarrow \Delta\Sigma_{ij} = \left(A_{ijkl}^{r} + A_{ijkl}^{\mathrm{m}}\right)\Delta\in_{kl}\end{aligned} \tag{14}$$

where C_{ijkl}^{m} is the fourth order compliance tensor of matrix. Finally, the yield criterion of the composite has been defined in such a way that it is equal to either of the phase yield criteria which goes to be first satisfied. In other words, the yield criterion of a two-phase system is introduced as follows:

$$F\left(\sigma_{ij}^{\mathrm{m}}, \sigma_x^r\right) = \max\left\{f^{\mathrm{m}}\left(\sigma_{ij}^{\mathrm{m}}\right), f^r\left(\sigma_x^r\right)\right\} \le 0 \tag{15}$$

The formula above indicates that the composite strength reaches the ultimate value when yielding takes place in both phases.

2.4. Stress Mohr circles evolution

Before improving the model by considering the interface effect, the behavior of a two-phase system is explained schematically in the space of stress Mohr circles. For instance, consider a two-phase element being under constant horizontal minor ($\Sigma_1 = cte$) and vertical major (Σ_2) principal stress field. The reinforcement phase is laid with an inclined angle of α from horizontal direction. The stress Mohr circles of both phases are sketched in Fig. 2. Since there is no

shear stress over the sample, we have: $\Sigma_{12} = \sigma^{m}_{12} + \sigma^{r}_{12} = 0$. In addition, due to the constant lateral stress, the sum of σ^{m}_{11} and σ^{r}_{11} remains constant, i.e., $\Sigma_1 = cte = \sigma^{m}_{11} + \sigma^{r}_{11}$. The sample is loaded by vertical uniform displacement which causes lateral deformation in the sample. As a result, the axial strain in the reinforcement enhances the tensile reinforcement stress (with negative sign) which makes the Mohr circle of the matrix move ahead on condition that two aforementioned equalities hold true during loading. Sequential numbers illustrate the process of the circle movement.

The growth of stress in and thus the movement of Mohr circle of the matrix totally depend on the reinforcement deformability. The initial stress condition is shown by circle no. 1. If the reinforcement has high stiffness (Fig. 2a), axial stress in reinforcement grows rapidly and moves the matrix circle to a long distance. This movement leaves off when the reinforcement circle touches its yield criterion line, whilst the matrix does not become plastic yet (circle no. 4). At this moment, it is the matrix that is alone under applied load and the circle gets bigger until it reaches the matrix yield criterion line too (circle no. 5).

In contrast with the previous case, consider the condition where the reinforcement has high extensibility (low stiffness). The stress in the reinforcement grows in a gentle manner so that the stress Mohr circle of matrix reaches the yield criterion at first (circle no. 3), whilst the reinforcement has not yet got plastic. By having successive lateral deformation in the sample, the axial stress in reinforcement continues to increase which again causes to move forward the Mohr circle of matrix, provided that all circles remain tangential to the yield criterion line as shown in Fig. 2b. The sample finally reaches the ultimate state when the reinforcement gets plastic too (circle no. 4).

3. Implementation of the interface effect in the two-phase model

As can be figured out from diverse trends in the behavior explained above, a two-phase system fails only if both phases reach their ultimate stress state (also refer to Eq. (15)). This is, however, against the cases observed in laboratory and field tests, in which a failure mechanism is generated in the reinforced soil mass without failure in both inclusion and soil (e.g., Broms, 1977; Cividini, 2002; Haeri et al., 2000; Holtz et al., 1982; Latha and Murthy, 2007; Tatsuoka and Yamauchi, 1986). In other words, it is the interaction between these constituents that fails and hence, the soil is not anymore supported by the inclusion.

In the present contribution, the interaction between phases is considered through a rigid-perfectly plastic contact; it is suggested that the stress in the reinforcement phase be limited by maximum admissible shear stress in the matrix phase along the reinforcement phase direction. By assuming that this surface has frictional resistance, the interrelation between phases will be interrupted if the tangential stress in this direction exceeds frictional strength. The interface failure function (f^{int}), described by Coulomb criterion, is expressed as follows:

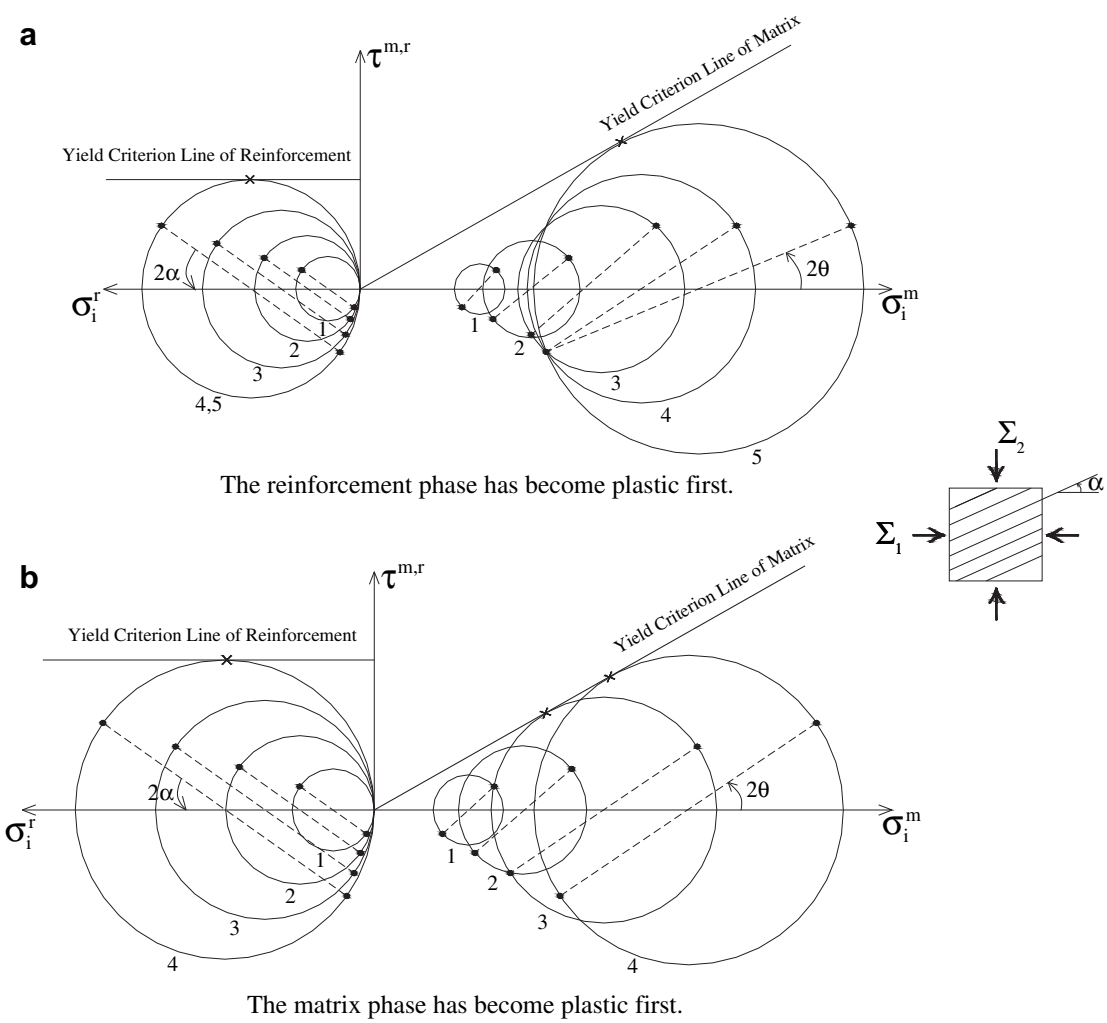

Fig. 2. Evolution of Mohr stress circles in matrix and reinforcement phases (perfect bonding).

$$f^{\mathrm{int}}(\tau,\sigma_{\mathrm{n}}) = \tau - \tan(\delta)\sigma_{\mathrm{n}} \tag{16}$$

where τ and σ_{n} are shear and normal stresses, in the matrix phase, corresponding to the interface surface direction. δ is the interfacial friction angle.

In order to calculate stress components $(\tau,\sigma_{\mathrm{n}})$, stress vector on the interface (t_i^{int}) is first assessed by having the normal direction of reinforcement plane with unit vector n_i:

$$t_i^{\mathrm{int}} = \sigma_{ij}^{\mathrm{m}} n_j = \begin{Bmatrix} -\sin\alpha\sigma_{11}^{\mathrm{m}} + \cos\alpha\sigma_{12}^{\mathrm{m}} \\ -\sin\alpha\sigma_{12}^{\mathrm{m}} + \cos\alpha\sigma_{22}^{\mathrm{m}} \end{Bmatrix} \tag{17}$$

where unit vector n_i equals:

$$n_i = \begin{Bmatrix} -\sin\alpha \\ \cos\alpha \end{Bmatrix} \tag{18}$$

The angle α is the reinforcement phase inclination from horizontal. Hence, by calculating the normal stress along unit vector n_i:

$$\sigma_{\mathrm{n}} = t_i^{\mathrm{int}} n_j = \sigma_{11}^{\mathrm{m}}\cos^2\alpha + \sigma_{22}^{\mathrm{m}}\sin^2\alpha - 2\sigma_{12}^{\mathrm{m}}\cos\alpha\sin\alpha$$

it is now possible to find the shear stress on the plane as follows:

$$\tau = \sqrt{|t_i^{\mathrm{int}}|^2 - \sigma_{\mathrm{n}}^2} \tag{19}$$

where $|t_i^{\mathrm{int}}|$ indicates the scalar value of the stress vector.

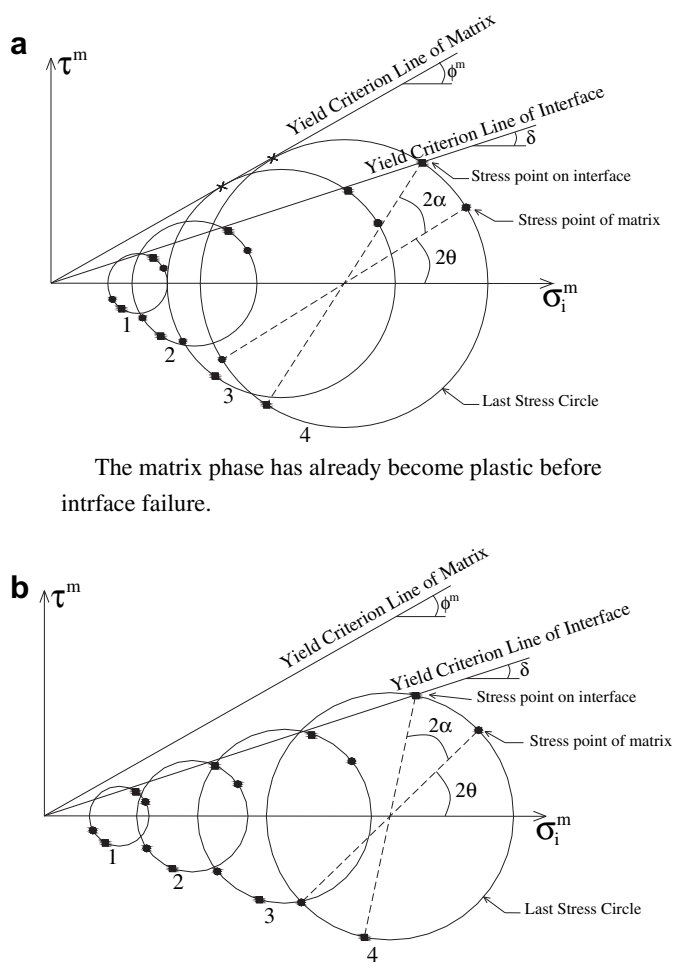

Fig. 3. The influence of interface on evolution of Mohr stress circles in the matrix phase.

Fig. 3 describes schematically the role of the interface in limiting the matrix stress growth in the space of Mohr stress circles. The interface can influence the global strength of a two-phase system in two different manners whether or not the matrix reaches its yield criterion line before the interface has failed. As shown in Fig. 3a, if the matrix becomes plastic first, the movement of Mohr circles, while being tangential on the yield criterion line, is halted when the stress point correspondent to the stress state on the interface surface coincides with the interface yield criterion line. On the contrary, in accordance with Fig. 3b, this is the interface that fails first and as a result, the matrix cannot reach its yield criterion line (circle no. 4).

In the latter case, the composite demonstrates a yield-like condition due to failure of interface. Hence, it may be regarded as if the composite contained a new soil material with weaker strength, i.e., smaller internal friction angle (ϕ^{int}). Besides, according to Rowe's stress–dilatancy theory (Rowe, 1962), the deformation mechanism in such a material corresponds to the characteristics of the failure surface, i.e., the interface dilatancy angle (ψ^{int}). The pseudo friction angle of the matrix can be assessed by having the angles α, θ, and δ as follows:

$$\phi_{\mathrm{int}}^{\mathrm{m}} = \sin^{-1}\left(\frac{\tan(\delta)}{\sin 2(\alpha+\theta) - \tan(\delta)\cos 2(\alpha+\theta)}\right) \tag{20}$$

The angle θ indicates the rotation of principal stress axes in the matrix phase:

$$\theta = \frac{1}{2}\sin^{-1}\left(\frac{\sigma_{12}^{\mathrm{m}}}{\sqrt{\left(\sigma_{22}^{\mathrm{m}} - \sigma_{11}^{\mathrm{m}}\right)^2/4 + \sigma_{12}^{\mathrm{m}2}}}\right) \tag{21}$$

Hence, plastic behavior of the matrix is modified, by replacing friction and dilatancy angles, as follows:

$$\begin{aligned} f^{\mathrm{m}}(\sigma_I^{\mathrm{m}},\sigma_{II}^{\mathrm{m}}) &= (\sigma_I^{\mathrm{m}} - \sigma_{II}^{\mathrm{m}}) - \sin\phi^{\mathrm{eq}}(\sigma_I^{\mathrm{m}} + \sigma_{II}^{\mathrm{m}}) \\ \phi^{\mathrm{eq}} &= \min\left\{\phi^{\mathrm{m}},\phi^{\mathrm{int}}\right\} \end{aligned} \tag{22a}$$

$$\begin{aligned} g^{\mathrm{m}}(\sigma_I^{\mathrm{m}},\sigma_{II}^{\mathrm{m}}) &= (\sigma_I^{\mathrm{m}} - \sigma_{II}^{\mathrm{m}}) - \sin\psi^{\mathrm{eq}}(\sigma_I^{\mathrm{m}} + \sigma_{II}^{\mathrm{m}}) \\ \psi^{\mathrm{eq}} &= \begin{cases} \psi^{\mathrm{m}} & \text{for } \phi^{\mathrm{m}} < \phi^{\mathrm{int}} \\ \psi^{\mathrm{int}} & \text{for } \phi^{\mathrm{m}} \geq \phi^{\mathrm{int}} \end{cases} \end{aligned} \tag{22b}$$

The equations above indicate that the plastic behavior of the matrix phase can be changed directionally as a function of stress state in the matrix phase as well as reinforcement phase inclination.

4. Numerical implementation

The proposed formulation is implemented in the finite difference-based code FLAC (Itasca Consulting Group, 2001). Since two types of material exist in each element, stress–strain calculation is performed separately for each phase. It is firstly assumed that applied total strain increment on the two-phase system is elastic. Therefore, elastic trial stresses in both phases are calculated. Then, it is examined if the stresses violate yield criteria. If the stress state lies outside its yield function, stress state is corrected by plastic correction procedure used in FLAC (explicit procedure). The calculation is initially launched for the matrix phase. In each step, the yield and potential functions are updated in accordance with Eq. (22). The calculation then continues for the reinforcement phase. If the interface has failed (i.e., $\phi^{\mathrm{int}} \leq \phi^{\mathrm{m}}$), no stress state is updated. Otherwise, the stress state is calculated according to stress–strain relationship and failure condition of the reinforcement phase.

5. Evaluation and verification

The study explained in this section includes three groups of numerical simulations. The first refers to the response of a plane strain compression test on a reinforced soil sample. The second concerns the deformation pattern of the face of a reinforced soil retaining wall and the numerical simulations are compared with experimental data. Finally, the behavior of a reinforced soil wall is simulated under its own weight and it is compared with the analysis result of another advanced homogenization method.

5.1. Simulation of a plane strain compression test

McGown et al. (1978) performed several plane strain compression tests on reinforced sand samples under confining pressure of 70 kPa. The soil used was dense Leighton Buzzard sand with relative density of 65%. Two different types of inclusions including aluminum foil and non-woven geotextile (T140) were applied. The aluminum foil had the stiffness (J) of 560 kN/m with tensile strength force (T^{u}) of 3 kN/m. The properties of geotextile were $J = 30$ kN/m and $T^{u} = 1.4$ kN/m. The dimension of reinforced soil samples was 152 mm × 102 mm × 102 mm. In all reinforced samples, one layer of inclusion was placed in the middle of the specimen with an inclined direction varying between $\alpha = 0$ and 90°. The samples were loaded vertically by rigid platen displacements, while the lateral stress was kept constant during the test. The sand parameters are estimated from the stress–strain graphs: $\varphi^{m} = 51°$, $\psi^{m} = 20°$, $E^{m} = 52$ MPa, and $\nu^{m} = 0.3$. No data were reported for the mechanical behavior of the interface. Hence, the value of the interface friction angle (δ) in the simulations is assessed to be 49° by trial and error procedure. It should be mentioned that the very thin layer of the reinforcing layer (about 8 μm for aluminum foil) would be deformed under compression of sand particles during sample preparation. Consequently, this high value for δ would be reasonable.

The sample is modeled as a single degree-of-freedom two-phase element under Σ_1 and Σ_2 principal stresses. In Fig. 4, the result of simulations without/with considering the failure interface is presented in terms of Maximum Stress Ratio (MSR), defined as $(\Sigma_2/\Sigma_1)_{max}$, along with inclination of inclusion. In the same figure, the result from experimental tests is demonstrated too. The comparison shows the influence of the interface resistance on the reinforced soil strength.

According to Fig. 4, it can be observed that MSR obtained from the simulation has the same trend as that of the experiment along with the inclination angle of the inclusion when the inclusion is inclined in a shallow angle from horizontal ($\alpha < 50°$). In this case, the composite strength is higher than that of soil alone; however, passing through $\alpha = 50°$, MSR becomes even smaller than that of non-reinforced sand. This reduction in MSR can only be predicted by the model in which the interface failure takes place.

5.2. Response of a reinforced retaining wall under external loading

Schiavo et al. (2001) have studied the behavior of a 1-g geogrid reinforced retaining wall model (Fig. 5a). The retaining wall face was made up of a set of rigid metallic strips hinged each other and kept vertically only by the interposition of geogrids. The geogrids (110 cm long) were placed in seven layers. The sand layers were prepared by raining technique with a relative density of 85% (unit weight = 16 kN/m^3). The reinforced retaining wall was loaded

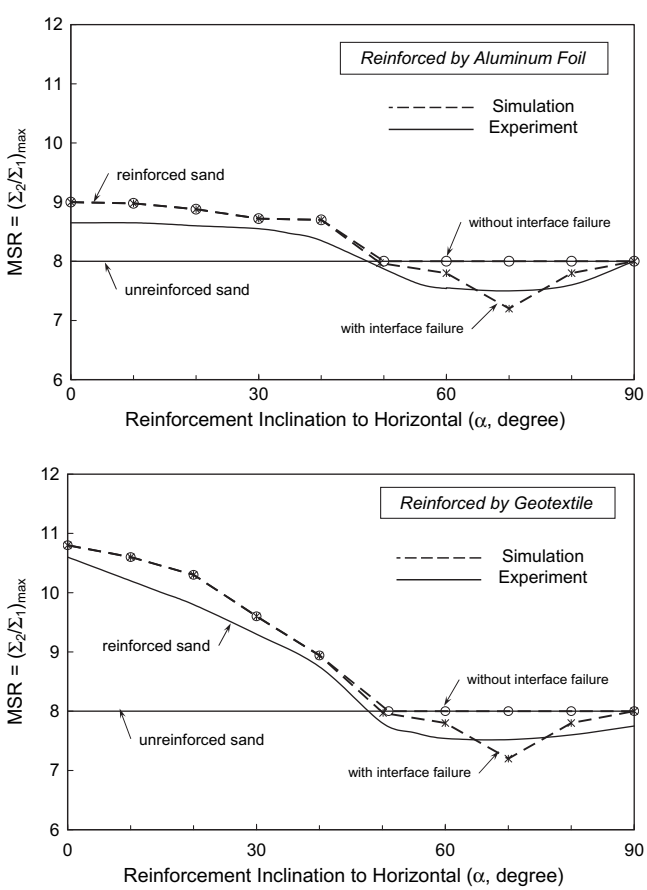

Fig. 4. Comparison of experimental and simulated behavior of reinforced soil samples in term of Maximum Stress Ratio (MSR) along with the inclusion inclination.

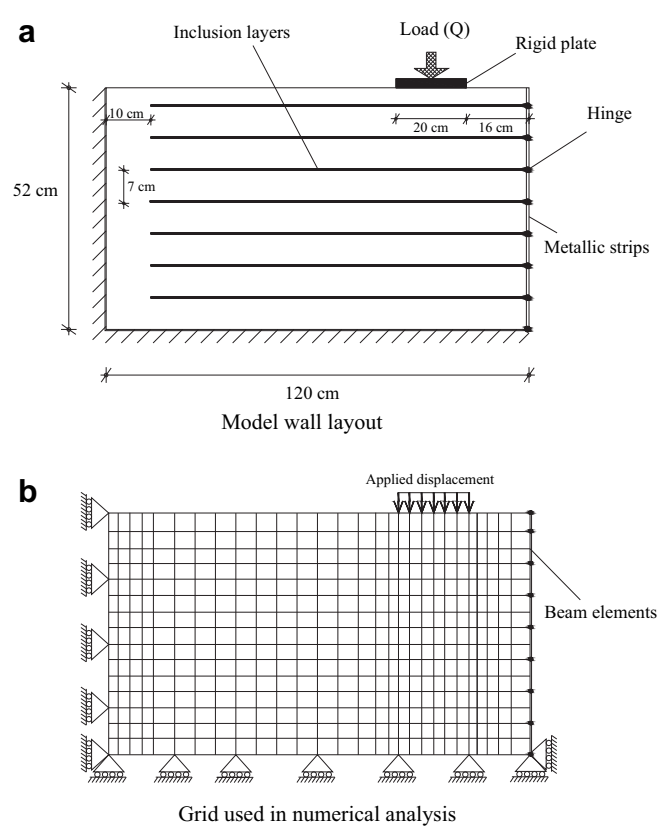

Fig. 5. Scheme of the reinforced soil retaining wall model under external loading.

through a rigid steel plate (200 mm × 400 mm) resting on top of the deck surface. Five horizontal transducers measured the wall face movement during the loading process. They have simulated the wall behavior by the finite-element-based code Plaxis. Based on triaxial compression tests on sand samples as well as the back-analysis of the experimental data for the wall deformation, they have proposed the following sand parameters: $\varphi = 42°$, $\psi = 9°$, $E = 6.5$ MPa, and $\nu = 0.2$. The geogrid used has $J = 55$ kN/m, $\nu = 0.3$, and tensile strength force (T^{u}) of 4.5 kN/m.

This problem is analyzed with the aid of multiphase concept in the present study by considering different interface behaviors. In the first analysis, the phases are perfectly bonded to each other (without interface failure). The analysis with Plaxis has been performed with the same condition where the soil and inclusions were modeled individually. Second analysis concerns the simulation of the wall behavior in which the interface failure is taken into account in the system. A value of $\delta = 34°$ and $\psi^{int} = 5°$ is chosen for the interface properties. The grid used and the boundary conditions in the analyses are shown in Fig. 5b.

Fig. 6 provides the wall face deformation measured in the test together with the result of simulations. First of all, by referring to Fig. 6a, it can be seen that there is a good agreement between the simulations of the homogenized and discrete (Plaxis) models. Secondly, by comparing Fig. 6a with Fig. 6b, it is found out that the proposed interface behavior has influence over the pattern of the face deformation. This influence becomes more evident as the applied load augments. The difference in the deformation pattern is highly distinguished in the upper half of the wall height. It is obvious that the deformation profile obtained from the model with the interface failure has more similarity with experimental data than the model with perfect bonding condition.

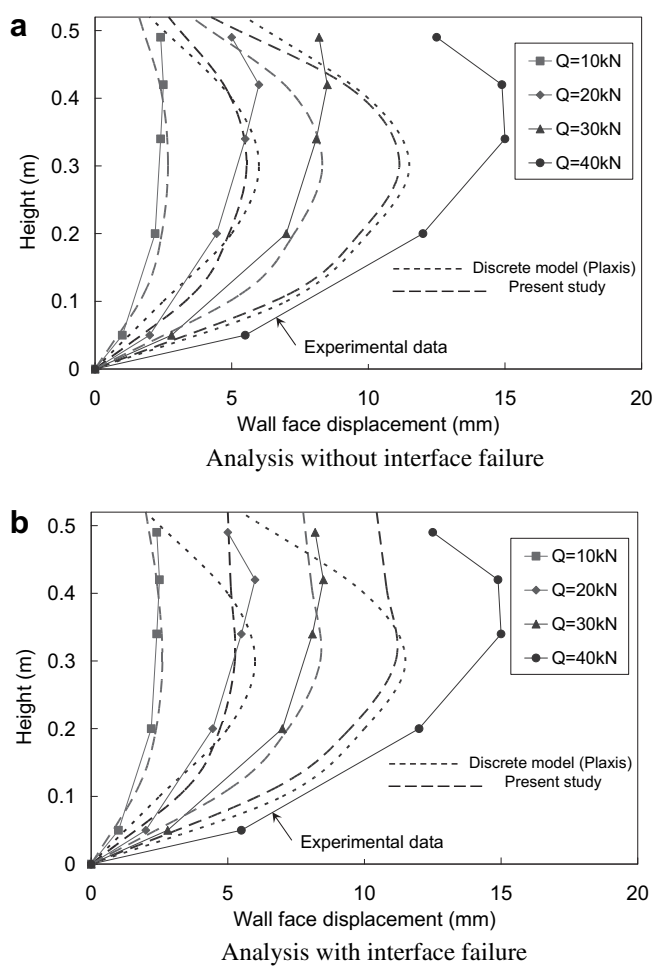

Fig. 6. Variation of horizontal wall face deformation at different load levels.

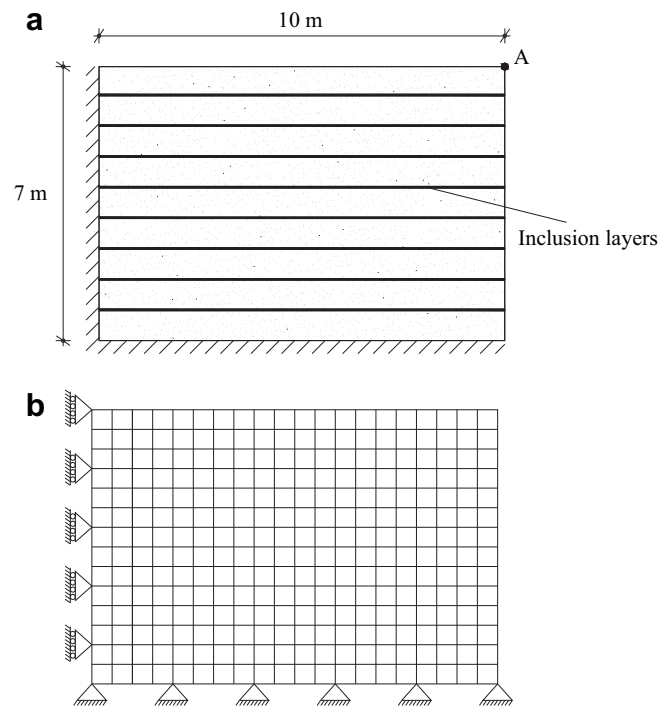

Fig. 7. Reinforced soil wall under its own weight: (a) global layout; (b) grid and boundary conditions used in numerical simulation.

5.3. Behavior of a reinforced soil wall under its own weight

Ensan and Shahrour (2003) have analyzed the deformation of a reinforced soil wall under its own weight by applying a constitutive model for multilayered materials in domain of homogenization theories. In their proposed model, the interface failure feature has been defined by considering relative displacement between the soil and the inclusion. The wall geometry is shown in Fig. 6a. The wall is composed of eight reinforcement layers with the properties as follows: $E^{inc} = 10{,}500$ MPa, $\nu^{inc} = 0.22$, and $\sigma_u^{inc} = 6$ MPa. The soil has the following characteristics: $\varphi^m = 30°$, $\psi^m = 30°$, $E^m = 150$ MPa, and $\nu^m = 0.3$. The analysis has been carried out by two values of interface friction angle $\delta = 10°$ and $20°$ (1/3 and $2/3\varphi^m$). In all analyses, $\psi^{int} = 4°$ has been assumed. The wall was loaded gradually by increasing the volume force from zero to the unit weight of the soil ($\gamma = 20$ kN/m^3) and the displacement of the upper corner point of the wall (point A in Fig. 7a) was calculated.

The same problems are analyzed here with the present model as a two-phase system. The grid used in the analysis is shown in Fig. 7b. The results of the analyses from both methods are depicted in Table 1. By comparing the results, it is interesting to find out that although the relative displacement is neglected in the present

Table 1
Horizontal displacement of point A obtained from different methods (mm).

Interface characteristics	Present model	Ensan and Shahrour (2003)
$\delta = 10°$	1.19	1.25
$\delta = 20°$	0.95	1.04
Perfect bonding	0.94	0.98

formulation, the obtained results are very similar to those of the other advanced model in which more extra parameters are needed for the interface.

6. Conclusion

In this paper, the interface effect in reinforced soil structures is taken into consideration as a rigid-plastic contact in two-phase systems. The analysis with the present model is simple and less time-consuming since there is no need to introduce a third phase and to calculate relative displacement between matrix and reinforcement phases.

By simulating the behavior of reinforced soil samples as a single element, the influence of interface failure on the global strength is clearly demonstrated. Then, by simulating the behavior of a 1-g reinforced soil wall model under external loading, it has been shown that in comparison with the perfect bonding model, the face deformation profile can be predicted more accurately by the present model.

Ignoring the relative displacement between soil and inclusion before interface failure in the proposed model might impose an error on predicting the deformation of reinforced soil walls. However, in the cases where the wall is not heavily loaded or it is under its own weight, it is found out that the error is small and ignorable. This is examined by investigating the simulated behavior of the above-mentioned model test as well as comparing the simulation result of a reinforced soil wall with that of the other homogenization method including elastoplastic interface model.

The efficiency of the proposed formulation in predicting the deformation of reinforced soil walls has been demonstrated in the present study. However, more investigation is required to examine the applicability of the model for stability analysis of reinforced soil structures.

References

Ben Hassine, W., Hassis, H., de Buhan, P., 2008. A macroscopic model for materials reinforced by flexible membranes. Mechanics Research Communications 35 (5), 310–319.

Bennis, M., de Buhan, P., 2003. A multiphase constitutive model of reinforced soils accounting for soil-inclusion interaction behavior. Mathematical and Computer Modeling 37, 469–475.

Broms, B.B., 1977. Triaxial tests with fabric reinforced soil. In: Proc. Int. Conf. on the Use of Fabrics in Geotechnics, 3, Ecole Nationale des Ponts et Chaussées, Paris. pp. 129–134.

Cazzuffi, D., Picarelli, L., Ricciuti, A., Rimoldi, P., 1993. Laboratory investigations on the shear strength of geogrid reinforced soils. Geosynthetic Soil Reinforcement Testing Procedures, ASTM STP 1190.

Cividini, A., 2002. A laboratory investigation on the behavior of reinforced sand samples under plane strain and triaxial conditions. Soils and Foundations 42 (6), 23–39.

de Buhan, P., Mangiavacchi, R., Nova, R., Pellegrini, G., Salencon, J., 1989. Yield design of reinforced earth walls by a homogenization method. Géotechnique 39, 189–201.

de Buhan, P., Sudret, B., 1999. A two-phase elastoplastic model for unidirectionally-reinforced materials. European Journal of Mechanics A/Solids 18, 995–1012.

de Buhan, P., Sudret, B., 2000. Micropolar multiphase model for materials reinforced by linear inclusions. European Journal of Mechanics A/Solids 19, 669–687.

Ensan, M.N., Shahrour, I., 2003. A macroscopic constitutive law for elasto-plastic multilayered materials with imperfect interfaces: application to reinforced soils. Computers and Geotechnics 30, 339–345.

Haeri, S.M., Nourzad, R., Oskoorouchi, A.M., 2000. Effect of geotextile reinforcement on the mechanical behavior of sand. Geotextiles and Geomembranes 18, 385–402.

Harrison, W.J., Gerrard, C.M., 1972. Elastic theory applied to reinforced earth. Journal of Soil Mechanics and Foundations Division ASCE 98 (12), 1325–1345.

Hassen, G., de Buhan, P., 2005. A two-phase model and related numerical tool for the design of soil structures reinforced by stiff linear inclusions. European Journal of Mechanics A/Solids 24, 987–1001.

Hatami, K., Bathurst, R.J., 2005. Development and verification of a numerical model for the analysis of geosynthetic-reinforced soil segmental walls under working stress conditions. Canadian Geotechnical Journal 42, 1066–1085.

Hatami, K., Bathurst, R.J., 2006. Numerical model for reinforced soil segmental walls under surcharge loading. Journal of Geotechnical and Geoenvironmental Engineering 132 (6), 673–684.

Holtz, R.D., Tobin, W.R., Burke, W.W., 1982. Creep characteristics and stress–strain behavior of a geotextile-reinforced sand. In: Proc. of Second Int. Conf. on Geotextiles, Las Vegas. pp. 805–809.

Itasca Consulting Group, 2001. FLAC—Fast Lagrangian Analysis of Continua. Version 4.00, Minneapolis.

Kotake, N., Tatsuoka, F., Tanaka, T., Siddiquee, M.S.A., Yamauchi, H., 1999. An insight into the failure of reinforced sand in plane strain compression by FEM simulation. Soils and Foundations 39 (5), 103–130.

Latha, G.M., Murthy, V.S., 2007. Effects of reinforcement form on the behavior of geosynthetics reinforced sand. Geotextiles and Geomembranes 25, 23–32.

Matichard, Y., Thamm, B., Sere, A., 1992. Behavior of a geotextile reinforced earthwork under surface loading. In: Proc. of Seiken Symposium no. 11, Tokyo, Japan. pp. 117–130.

McGown, A., Andrawes, K.Z., Hasani, M.M., 1978. Effect of inclusion properties on the behavior of sands. Géotechnique 3 (28), 327–346.

Michalowski, R.L., Zhao, A., 1995. Continuum versus structural approach to stability of reinforced soil. Journal of Geotechnical Engineering Division ASCE 121, 152–162.

Peng, F.L., Kotake, N., Tatsuoka, F., Hirakawa, D., Tanaka, T., 2000. Plane strain compression behavior of geogrid-reinforced sand and its numerical analysis. Soils and Foundations 40 (3), 55–74.

Romstad, K.M., Herrmann, L.R., Shen, C.K., 1976. Integrated study of reinforced earth-I: theoretical formulation. Journal of Geotechnical Engineering Division ASCE 102 (GT5), 457–471.

Rowe, P.W., 1962. The stress–dilatancy relation for static equilibrium of an assembly of articles in contact. Proceedings of Royal Society London Series A 269, 500–527.

Seyedi Hosseininia, E., 2009. A Contribution to Development of Multiphase Model by Considering the Non-Linear Behavior of Matrix Applied to Geosynthetics-Reinforced Soil (GRS) Structures. PhD dissertation, University of Tehran, Tehran, Iran (in Persian).

Seyedi Hosseininia, E., Farzaneh, O., 2007. Development of multiphase model of reinforced soils considering non-linear behavior of the matrix. In: Proc. of 5th International Symposium on Earth Reinforcement, Fukuoka, Japan.

Seyedi Hosseininia, E., Farzaneh, O., 2008. Presentation of a homogenized multiphase model for reinforced soil considering non-linear behavior of matrix. In: Proc. of the 12th Int. Conf. of Int. Assoc. for Comp. Meth. and Adv. in Geomech. (IACMAG), Goa, India.

Schiavo, M., Simonini, P., Gottardi, G., Tonni, L., 2001. Use of a 1g geogrid reinforced-wall model to evaluate the effectiveness of a FE numerical code. In: Landmarks in Earth Reinforcement: Proc. of the Int. Symposium on Earth Reinforcement, Fukuoka, Kyushu, Japan.

Sudret, B., de Buhan, P., 2001. Multiphase model for inclusion-reinforced geostructure: application to rock-bolted tunnels and piles raft foundations. International Journal of Numerical and Analytical Methods in Geomechanics 25, 155–182.

Tatsuoka, F., 1985. On the angle of interface friction for cohesionless soils. Soils and Foundations 25 (4), 135–141.

Tatsuoka, F., Yamauchi, H., 1986. A reinforcing method for steep clay slopes with non-woven fabric. Geotextiles and Geomembranes 4 (3/4), 241–268.

Thai, S.Q., Hassen, G., de Buhan, P., 2009. A multiphase approach to the stability analysis of reinforced earth structures accounting for a soil-strip failure condition. Computers and Geotechnics 36, 454–462.